Performance improvement of new Swisens Classifier evaluated using AutoPollen Hirst Timeseries

Swisens AG

December 13, 2024

Abstract

This report presents the development and evaluation of a new classification algorithm for allergenic pollen detection using SwisensPoleno Mars and Jupiter systems. The new classifier leverages holography images and fluorescence spectra to achieve significant improvements in classification accuracy, particularly for key allergenic pollen taxa. Correlations with Hirst data increased by an average of 45.9%, with R^2 values exceeding 0.9 for most relevant taxa. Additionally, the classifier successfully reduced off-season false-positives and improved the differentiation between pollen and water droplets even further, addressing previous limitations. The scope of classified taxa and particles was significantly expanded, encompassing new pollen types, as well as fungal spores and other particles like mineral dust and sand. These enhancements provide a robust, scalable solution for accurate real-time pollen monitoring, paving the way for further advancements in automatic bioaerosol classification.

Contents

1 Introduction **3**
1.1 Model Description 3
1.2 Training Datasets 4
1.3 Hirst time series data 6
1.4 Fine-Tuning 6
1.4.1 Filtering 6
1.4.2 Supervisor 6
1.4.3 Scaling Factor 8
1.4.4 Water Suppression 8

2 Time series evaluation based on Hirst data **11**
2.1 Classifier performance for SwisensPoleno Jupiter: Holography and fluorescence spectra 11
2.2 Classifier performance for SwisensPoleno Mars: Holography 15

3 Off-Season Performance Improvements **18**

4 Summary and Conclusion **20**
4.1 Benefits of the new classifier 21

5 Outlook **21**

6 Acknowledgments **22**

1 Introduction

The SwisensPoleno is very reliable in continuously measuring particles such as pollen grains, fungal spores, mineral dusts, water droplets and many other particles in the environment. For automatic pollen monitoring, however, besides the characterization of pollen grains, the pollen taxa needs to be classified to report the concentrations of the correct taxa. Classifiers based on artificial intelligence are very powerful to identify image-based data, such as those generated by the SwisensPoleno in form of holography images [1]. However, the classification performance and the real world performance is greatly influenced by the classification model architecture used, the local diversity of bioaerosols, the datasets used for model training, the features determined by the measurement instrument (for example holography and fluorescence), as well as the post-processing steps applied before reporting concentrations. It has been shown that the performance of different classifiers can vary when applied to the same outdoor measurements [2].

This report outlines the methodology and results of training an AI-based classification model based on holography images and fluorescence spectra of pollen, fungal spores, mineral dusts and water droplets measured by SwisensPoleno. To show the classifier's improvement, its results are compared with the classification of the model deployed on each SwisensPoleno system by default. It was developed by the Federal Office of Meteorology and Climatology MeteoSwiss (furthermore referred to as *MeteoSwiss*) with the intention of being used in Switzerland. As such, it is fine-tuned to work for pollen relevant within Switzerland and its climate. It only uses holography images as input. For simplicity, we are referring to it as *MCH* model in this report. This report compares pollen types for which the results of the MeteoSwiss Classifier are available and which were fully in-season during the Hirst time series it is compared to. These are the pollen types Betula, Fraxinus, Pinus, Poaceae and Quercus.

1.1 Model Description

The combination of holography images and fluorescence spectra can greatly improve the classification performance [5]. Therefore, data of both measurement methods were used in the training of a new classifier by applying a transfer learning approach with an EfficientNet-based model architecture shown in Figure 1. Furthermore, this architecture also allows the use of holography data only, which ensures model compatibility for data measured by SwisensPoleno Jupiter and SwisensPoleno Mars.

The model combines two streams of data (fluorescence spectra and holography images) to classify particles into 25 categories. The fluorescence spectra are processed through convolutional layers, which extract important features like patterns or peaks, followed by flattening and fully connected layers to create a numerical (vector) representation of the extracted features. The holography images on the other hand are analyzed using EfficientNet B0 [4], a pre-trained model specialized in recognizing visual features. Its output is flattened to a feature vector. The two feature vectors (one from holography and one from fluorescence) are then combined and passed through several fully connected layers with normalization, dropout, and activation functions, which allow the model to refine the combined data and help to reduce overfitting. The final layer outputs the classification result, identifying which of the 25 particle types the data given to the

classifier belongs to.

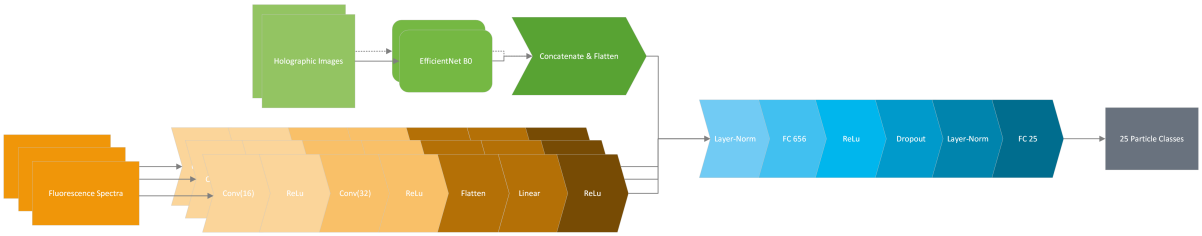


Figure 1: Model architecture: The new model processes both holography images, as well as all three fluorescence spectra (excitation sources: 280 nm, 365 nm and 405 nm), separately.

The classifications for data measured by SwisensPoleno Jupiter and Mars follow the same process, except for providing no fluorescence input (zero-values) to the classifier for SwisensPoleno Mars.

1.2 Training Datasets

The new classifier was trained on 687'154 particles from 97 datasets created on 16 different SwisensPoleno systems. The wide variety of training data sources reduces instrument-, operator- and location-specific biases of the new classifier. The full list of taxa used to train the new classifier can be found in table 1. Data cleaning was performed by the partners providing the datasets and differs between partners. These datasets were reviewed and potentially re-cleaned based on the distributions of class-specific key parameters such as size and shape. Datasets provided by Swisens followed a cleaning process which also includes UMAP [6] cluster analysis. The current best practice suggested by Swisens includes, but is not limited to, the removal of events

- with only one or no holography image
- with no particle(s) on images
- with blurry images
- with out-of-distribution size (area, diameter)
- with out-of-distribution shape (eccentricity, solidity)
- with no fluorescence spectra.

Please note that the cleaning process is currently neither quantitatively defined nor standardized.

Table 1: List of classes and particle types / taxa therein.

Class name	**Total number of events**	**Particle type/taxa in class**
Alnus	35'539	*A. glutinosa*, *Alnus* sp.
Ambrosia	29'233	*A. artemisiifolia*, *Ambrosia* sp.
Artemisia	46'763	*A. campestris, A. vulgaris,* *A. absinthum, Artemisia* sp.
Betula	49'239	*B. pendula, Betula* sp.
Corylus	78'219	*C. avellana, Corylus* sp.
Fagus	11'433	*Fagus sylvatica*
Fraxinus	22'454	*F. excelsior, F. ornus*
Cupressaceae	11'632	*Juniperus communis, Cupressus sempervirens*
Olea	10'941	*Olea europaea*
Ostrya	5'868	*O. carpinifolia, Ostrya* sp.
Parietaria	4'115	*P. officinalis*
Pinaceae	28'276	*P. pungens, P. abies, A. alba*
Pinus	39'674	*P. sylvestris, Pinus* sp.
Plantago	29'887	*P. lanceolata*
Poaceae	93'097	*D. glomerata, H. lanatus, A. pratensis,* *L. perenne, L. multiflorum, D. glomerata,* *T. flavescens, Anthoxanthum* sp., *Phleum* sp.
Populus	18'448	*P. nigra*
Quercus	27'617	*Q. robur, Q. petraea*
Salix	12'862	*S. alba, S. cinerea, Salix* sp.
Taxus	11'265	*T. baccata, Taxus* sp.
Urtica	40'863	*U. dioica, Urtica* sp.
Alternaria	18'633	*A. alternata*
Phytophthora	7'924	*P. infestans*
Mineral Dust	1'168	Illite-NX
Sand	17'329	Sand from concentrator
Water	34'675	Droplets of distilled water

1.3 Hirst time series data

Currently, the only reference for validation of automatic pollen and fungal spores monitoring are manually counted pollen concentrations sampled with Hirst-type traps [3]. During the COST ADOPT EUMETNET AutoPollen intercomparison campaign in Munich (furthermore referred to as *AutoPollen*), four Hirst traps were operated [2]. During the intercomparison campaign, the mean pollen concentration of the four traps was computed for the evaluation of the automatic instruments.[9]

The evaluation of the new classifier was done following the same procedure as in the AutoPollen intercomparison campaign in 2021. The raw time series data of the SwisensPoleno Jupiter instrument participating in the intercomparison campaign was used to evaluate the performance of the new classifier.

1.4 Fine-Tuning

The raw classification results for each particle, including the predicted class and classification confidence, are adjusted to ensure that the calculated concentrations closely match Hirst data collected with Hirst traps. This adjustment process is divided into two main steps: (I) filtering based on classification confidence and (II) verifying whether it is reasonable for a particle of a specific class to be detected (supervisor). Various combinations of filtering and supervisor settings are tested, aiming to minimize the number of particles excluded by the filtering while maximizing correlation with Hirst trap data. This approach ensures both accurate predictions and high sampling efficiency, which are essential for reliable pollen monitoring.

1.4.1 Filtering

In machine learning, a confidence value represents the model's estimated probability or certainty that its prediction is correct. It typically ranges from 0 to 1 (or 0% to 100%), where higher values indicate greater confidence in the prediction. For example, in a classification task, a model might predict a label and assign a confidence value indicating how sure it is about that prediction. These values are often used to filter predictions, prioritize outputs, or assess model reliability in real-world applications.

Here, it is used during fine-tuning to optimize the balance between false-positive rates and overall effectiveness. This process determines the minimum confidence threshold for each pollen type to accept a classification and include it in concentration calculations. Fine-tuning focuses on setting these thresholds to filter out low-confidence predictions, reducing unreliable classifications. By systematically adjusting the confidence thresholds for each pollen type, the optimum is identified to achieve high correlation with Hirst data, minimal scaling factors (¡15), and fewer off-season detections.

1.4.2 Supervisor

The supervisor is a post-processing step which prevents possible off-season false classifications to be counted [8]. It can be used during continuous-monitoring-operation such as measurement networks. It works independently of prior information such as the taxa specific pollen season, as it only relies on what the SwisensPoleno and the classifier are

detecting.

During the pollen season, a large number of pollen are measured each day. The confidence value of many classifications of these pollen will be very high. In contrast, outside the season, the confidence value of classifications of the same pollen type often times is lower.
The confidence filtering removes most of the wrongly classified particles by only trusting higher confidences, however, there are still a few particles mistakenly counted. During the season of a taxa, they account for a very small fraction of the total correctly counted pollen. However, outside of the season, where concentrations should be zero, these false classifications account for a major part of what is detected for a taxa and may lead to concentrations above zero. With the supervisor, off-season detection can be reduced or eliminated completely. It monitors the taxa-specific number of the last hours and, based on the evaluation results of the monitoring period, activates or deactivates the suppression of a pollen type for counting. The evaluation is done as follows: The supervisor enables classes for which a certain amount (*Event Counting (n)*) of high certainty (*High-Confidence Threshold (c)*) classifications has been detected over a specified time frame (*Time Integration (t)*). Otherwise, the class remains suppressed. When the season is over, the daily concentrations will decrease and the supervisor will automatically deactivate the class. This principle is demonstrated in Figure 2 and Figure 3.

High-Confidence Threshold (c): A secondary taxa-specific confidence threshold is defined that's significantly higher than the general taxa classification confidence threshold. This ensures that only particles with a high degree of classification confidence are considered.

Time Integration (t): The time window during which particle classifications with a high confidence c are counted. Usually it is set to 24 or 48 hours.

Event Counting (n): The number of particles with a high confidence c which need to be detected during the time t for one taxa, in order to enable a class. Only if the count exceeds this threshold, classified particles are counted toward the calculated concentration.

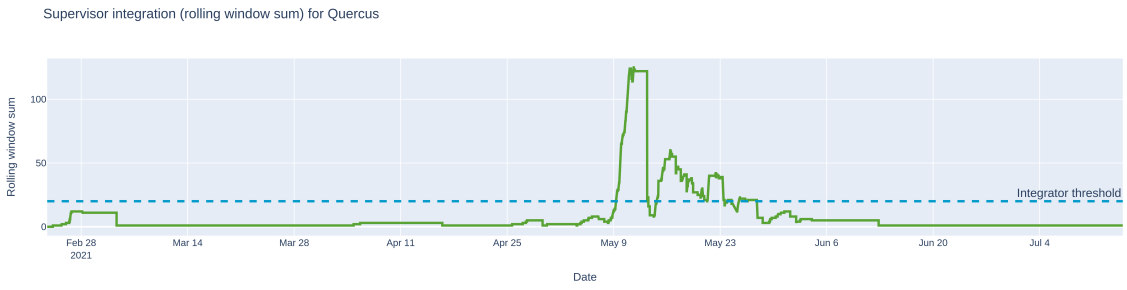


Figure 2: Example of the supervisor integrator for the Quercus class with the threshold of 20 particles (blue). Whenever the integrator of Quercus classifications in Figure 2 exceeds this value, the mask is set to 1, enabling the class. In this example, Quercus is enabled at the start start of its blooming season and disabled after.

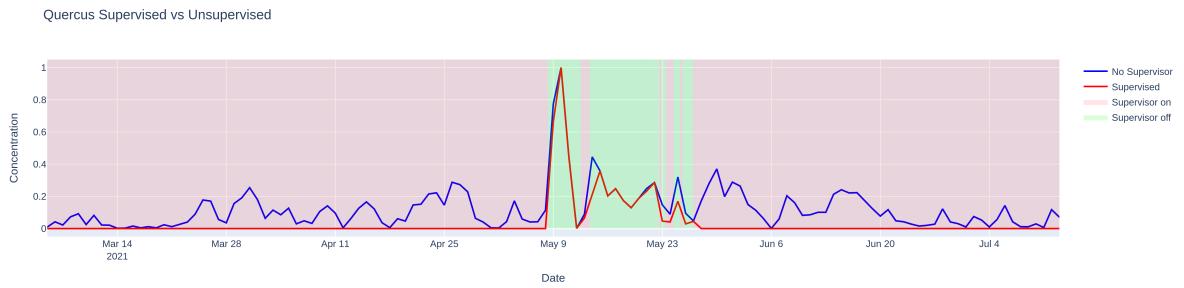


Figure 3: Example of the supervisor applied to the Quercus class with the settings t=48 hours, c=0.99999, n=20. The background-color in Figure 3 corresponds to the supervisor status (on: green; off: red). The suppression of off-season noise is clearly visible between March and April, as well as between June and July.

1.4.3 Scaling Factor

The scaling factor accounts for systematic losses arising in the sampling parts (inlet and sampling tube), in the detection system, in the classifier and finally from the confidence filtering. It is calculated per taxa by aligning the sum of all particles for a season with Hirst data. It allows a direct comparison of the concentration from SwisensPoleno instruments to the concentration from Hirst. The smaller the scaling factor is the better is the overall efficiency. The better the efficiency the smaller the uncertainty especially at low particle concentrations.

1.4.4 Water Suppression

The SwisensPoleno not only measures particles typically found in Hirst-type traps but also captures additional particle types. An important example is water in its various aggregate states, particularly water droplets, which are relevant to this report. Water droplets are nearly perfect spheres, typically ranging in size from $\sim 5\ \mu m$ to $30\ \mu m$. Notably, Poaceae (grass pollen) also falls within this size and shape category. Misclassifications of water droplets as Poaceae can lead to pronounced out-of-season signals. Even a low false-positive rate becomes problematic, as rain and mist generate a large number of detected particles.

Although water droplets and Poaceae are similar in size and shape, their fluorescence signals differ significantly. Water, when uncontaminated, emits no fluorescence, while Poaceae is one of the most fluorescent pollen types. Consequently, a classification algorithm incorporating fluorescence data should easily distinguish between these two classes. This section highlights the improvements introduced by the new algorithm in addressing this challenge.

Since its release, the existing 2022 model has struggled with significant false-positive classifications of water droplets as Poaceae. To mitigate this issue, the ***RainSuppressor*** system (WS) was developed. This system leverages a key observation: during rain or mist events, the ratio of false-positive Poaceae classifications to water droplet detections converges to a specific range — between 1:5 and 1:50. A simple rule suppresses false-positive Poaceae classifications by detecting such rain events and responding appropriately. As a

result, the system can detect rain events and react accordingly by ignoring false-positive Poaceae classification.

The effectiveness of this system depends on the Poaceae-to-water-droplet ratio rapidly reaching and maintaining the defined threshold during rain or mist events. Ideally, an algorithm should react quickly to such events (fast response) and provide a clear signal (large ratio). Using this metric, we can evaluate an algorithm's susceptibility to falsely report Poaceae pollen, even with the rain suppressor in place.

The new algorithm demonstrates strong performance in this regard. However, the practical benefits of the rain suppressor could not be assessed using AutoPollen time series data, as no significant rain periods with Poaceae misclassifications were recorded. Instead, performance was evaluated on a SwisensPoleno instrument in central Switzerland during a substantial rain and mist period.

Figures 4 and 5 summarize the performance improvements. Figure 4 shows the number of Poaceae particles detected per water detection, where lower values are better. Although the average and median values of the new classifier are only slightly lower, it significantly reduces outliers. Outliers can prevent the rain suppressor system from detecting rain events, resulting in false Poaceae measurements. Even with the rain suppressor enabled, the outliers persist in the existing classifier from MeteoSwiss (labeled MCH).

To illustrate the real-world implications, Figure 5 presents the false-positive rates across four scenarios. This figure underscores the effectiveness of the rain suppressor system. For the MCH model, the system eliminates 92.3% false-positives, while for the new classifier (labeled SWS), where the ratios are more stable, it achieves an impressive 99.92%. Notably, no additional tuning or adjustments were made to the suppression system for the SWS model.

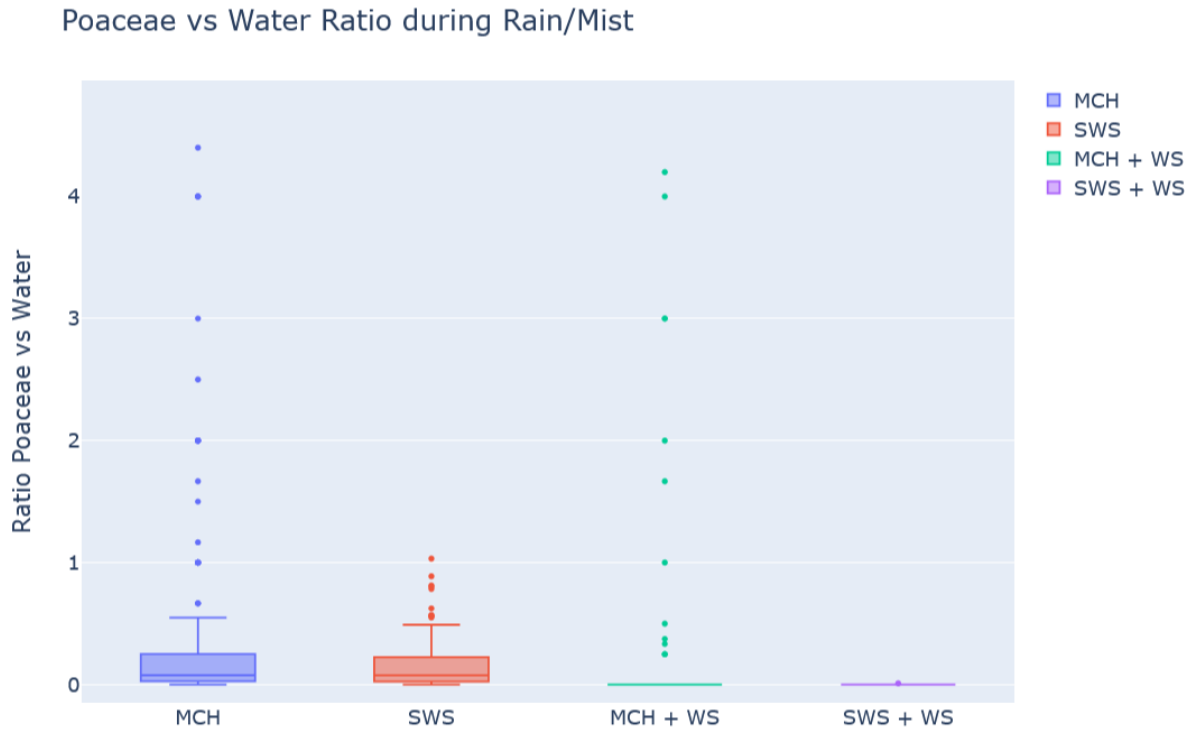


Figure 4: Ratio of Poaceae detections vs water detections during a rain event. Lower is better, as it represents a better Signal-to-Noise Ratio (SNR). Using the water suppressor (WS), the ratio approaches zero, which is the desired outcome. Note the outliers when combining the MCH model with the WS system. These outliers are no longer present using the new SWS model with the WS system Data source: SwisensPoleno Jupiter, Emmen, Switzerland, November 2024.

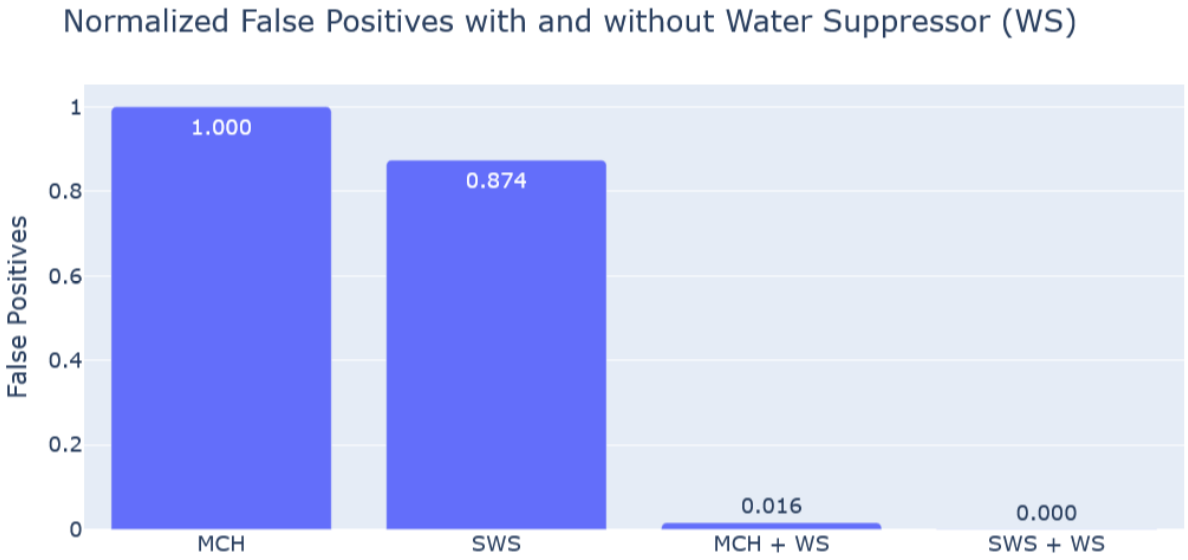


Figure 5: Relative false-positive rate with and without the water suppression system enabled for the SWS and MCH models. Smaller is better. Zero indicates no false-positives. SwisensPoleno Jupiter, Emmen, Switzerland, November 2024.

2 Time series evaluation based on Hirst data

The measurement data of the SwisensPoleno evaluated in this section comes from the COST ADOPT EUMETNET AutoPollen intercomparison campaign in Munich 2021 where multiple automatic pollen monitors and classifiers were compared [2]. This campaign provides reliable data from Hirst, as four Hirst traps where used in parallel to reduce the uncertainty [9]. As such, it provides a good ground to evaluate the new classifier.

Evaluations of the classifier were distinguished between SwisensPoleno Jupiter, where input data of both holography and fluorescence were used, and SwisensPoleno Mars where only holography images were used. However, the data was collected with a SwisensPoleno Jupiter and SwisensPoleno Mars was mimicked by discarding fluorescence data. The classifier running on SwisensPoleno instruments by default was developed by the Federal Office of Meteorology and Climatology MeteoSwiss (furthermore referred to as *MeteoSwiss*) specifically for Switzerland. It only uses holography images as input. For simplicity, we are referring to it as "*MCH*" model in this report. The default confidence thresholds and supervisor parameters developed for its use in Switzerland are applied.

2.1 Classifier performance for SwisensPoleno Jupiter: Holography and fluorescence spectra

The direct comparison of the new classifier (in this report referred to as *SWS*) with the existing classifier from MeteoSwiss (Figure 6, Table 2) shows a significant increase of correlation with Hirst data despite the increase in complexity caused by the addition of new classes and fluorescence spectra (table 1). This is driven by the reduction of off-season noise with the new classifier as can be seen for Quercus.The filters and supervisor configurations listed in 2 refer to the SWS model.

Table 2: Time series performance per class (with supervisor) for SwisensPoleno Jupiter (Holography and fluorescence spectra)

Class	**Filters**	**Supervisor configuration**	**SWS**		**MCH**	
			R	**R²**	**R**	**R²**
Betula	confidence: 0.995	c=0.995, t=2880 min, n=10	0.97	0.93	0.83	0.68
Fraxinus	confidence: 0.9	c=0.99, t=720 min, n=30	0.96	0.92	0.92	0.85
Pinus	confidence: 0.6	c=0.99999, t=720 min, n=20	0.97	0.94	0.97	0.94
Poaceae	confidence: 0.9	c=1, t=1440 min, n=1	0.97	0.95	0.79	0.62
Quercus	confidence: 0.9	c=0.99, t=720 min, n=30	0.93	0.86	0.31	0.11

Below, the individual time series for which reliable Hirst is available can be seen. The concentrations are reported after applying confidence-thresholding and the supervisor.

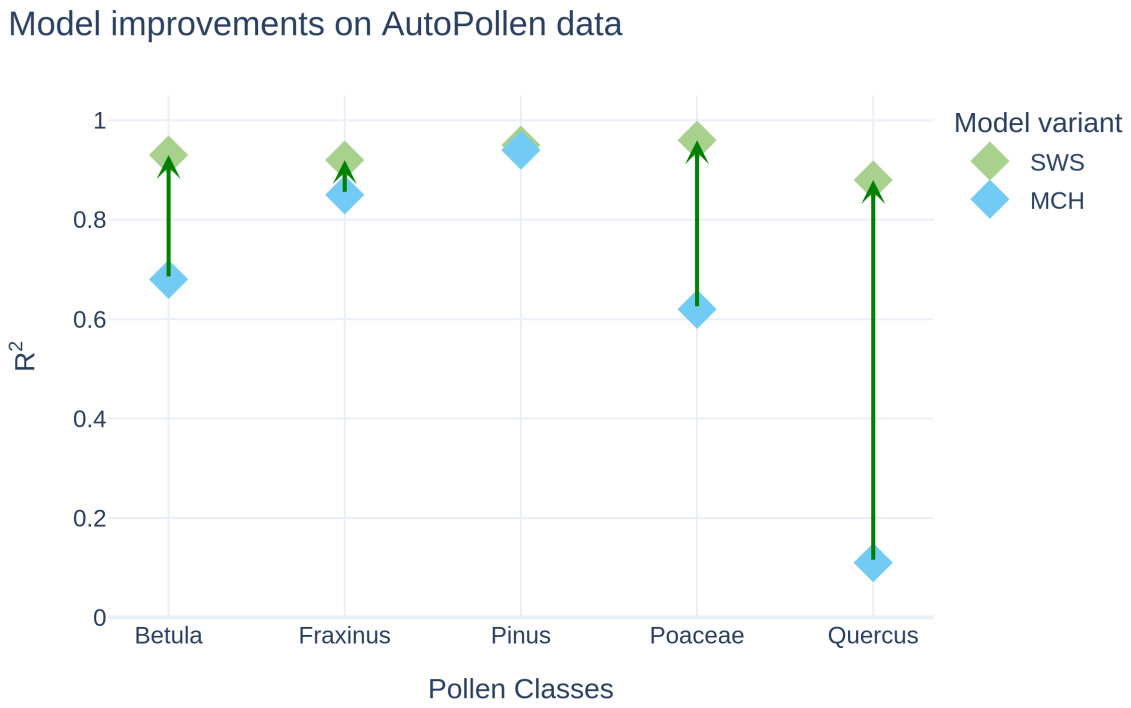


Figure 6: The new classifier provides significant improvements over the existing classification model for SwisensPoleno (Holography).

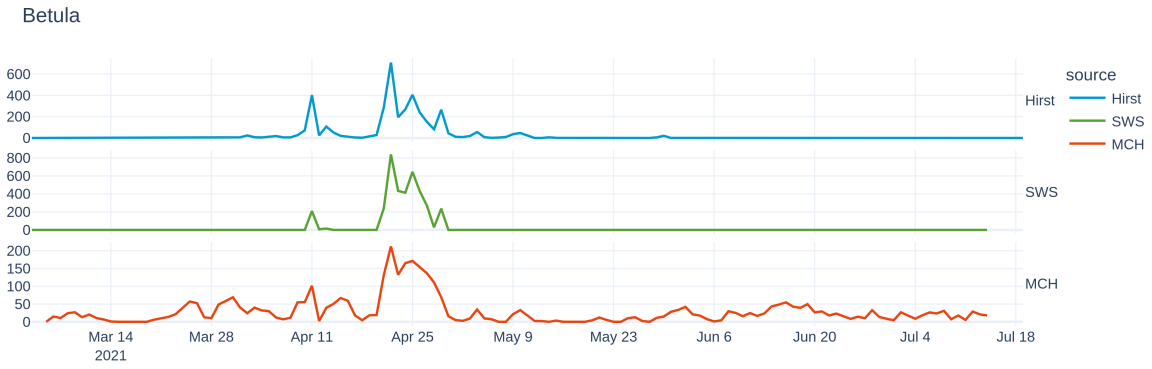


Figure 7: Betula R^2: 0.93; Betula shows very good correlation with Hirst data. This was achieved by the reduction of off-season noise.

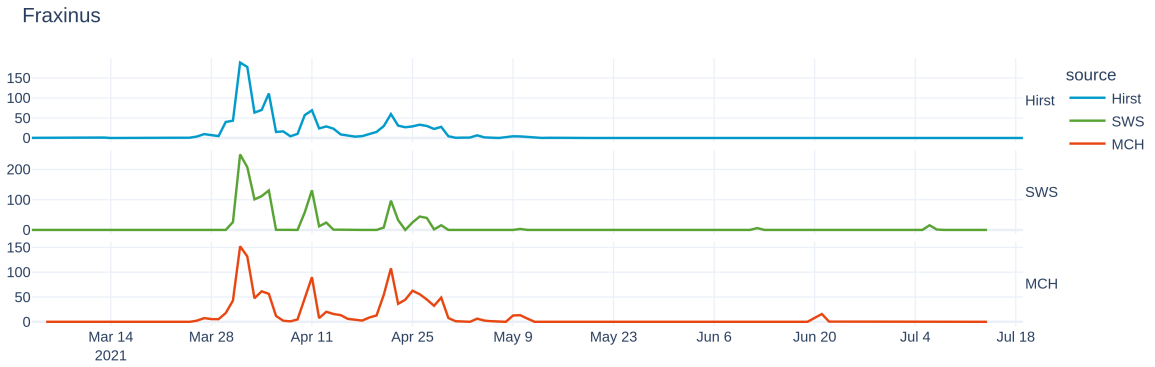


Figure 8: Fraxinus R^2: 0.92; Fraxinus shows very good correlation with Hirst data and reduces the late-April spike to similar levels as Hirst.

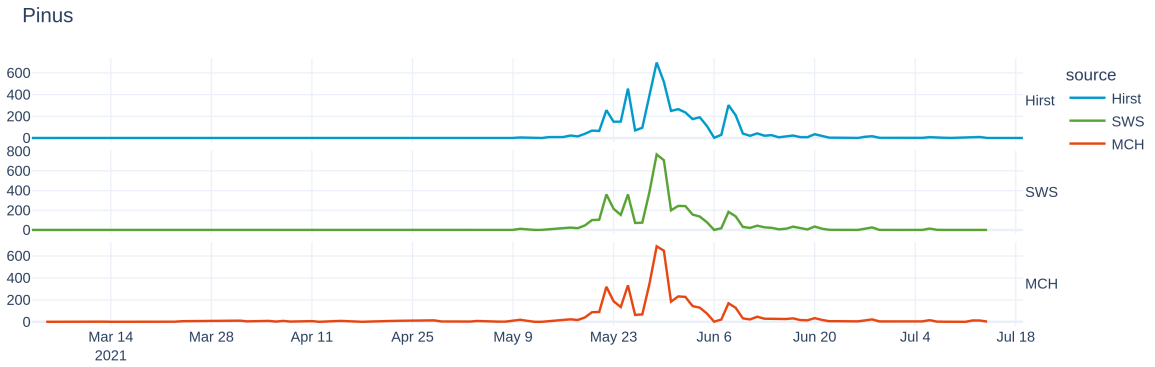


Figure 9: Pinus R^2: 0.94; Pinus shows very good correlation with Hirst data.

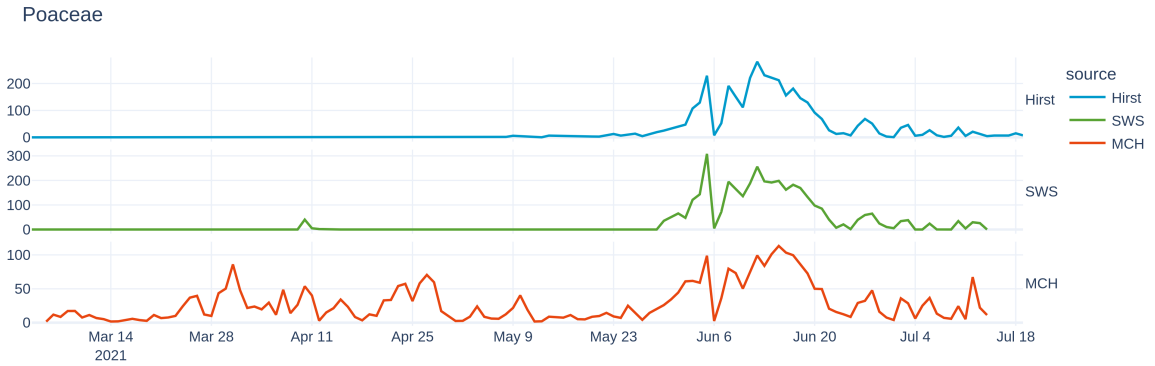


Figure 10: Poaceae R^2: 0.95; Poaceae shows very good correlation with Hirst. Few offseason peaks can be detected during April.

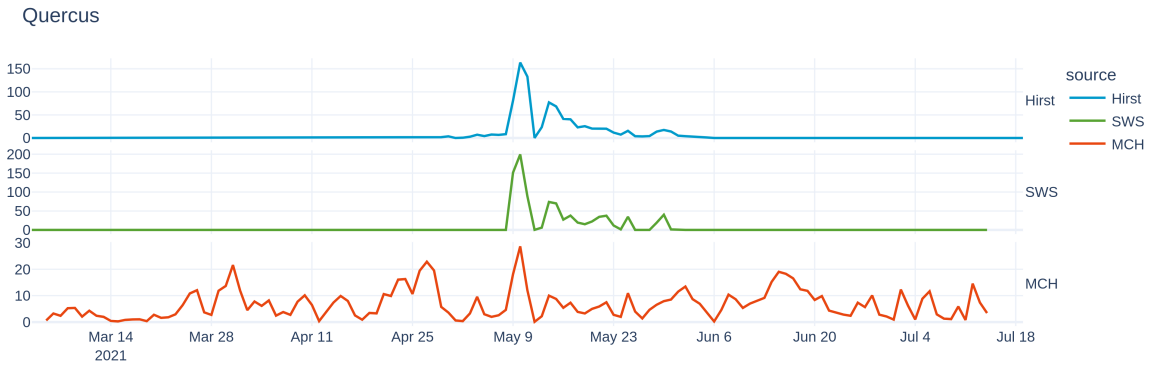


Figure 11: Quercus R^2: 0.86; Quercus shows very good correlation with Hirst data due to the reduced off-season noise.

2.2 Classifier performance for SwisensPoleno Mars: Holography

The model's ability to work without fluorescence spectra was evaluated on the same AutoPollen time series data, but only using the holography images as input. This simulates the classifier's performance on SwisensPoleno Mars systems. Again, the new classifier shows significant increases in correlation with Hirst data.

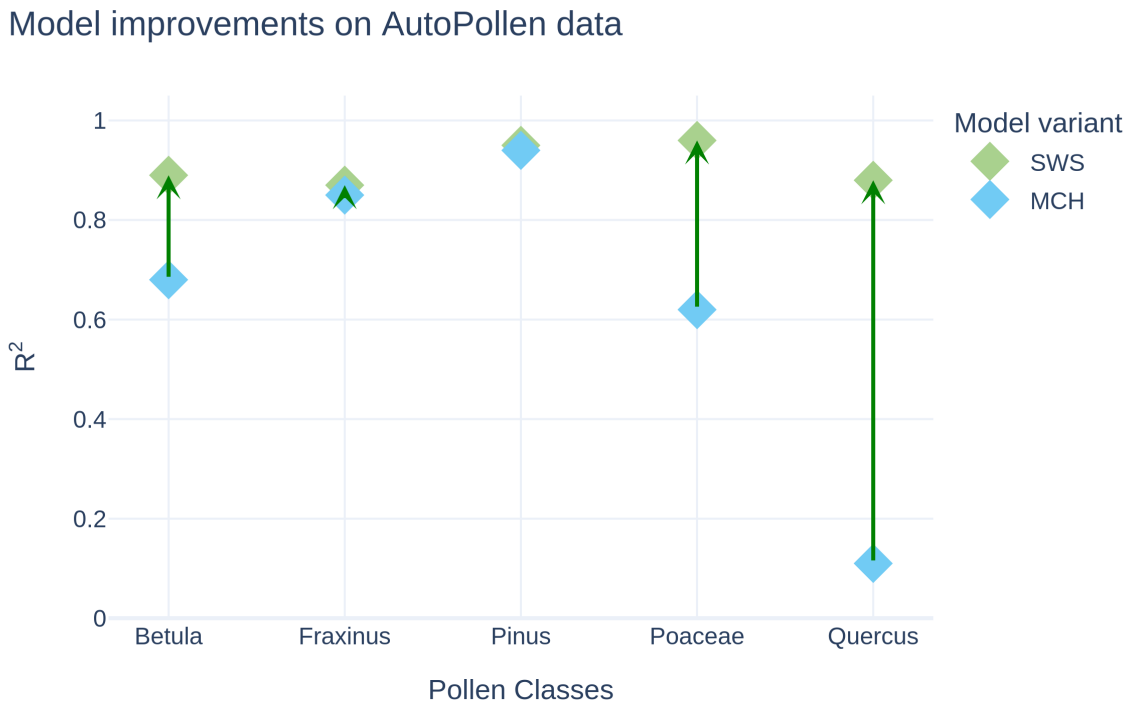


Figure 12: The new classifier based on holography data provides significant improvements over the existing classification model.

Table 3: Time series performance per class (with supervisor) for SwisensPoleno Mars (Holography)

Class	Filters	Supervisor configuration	SWS		MCH	
			R	R^2	R	R^2
Betula	confidence: 0.995	c=0.999999, t=720 min, n=5	0.94	0.89	0.83	0.68
Fraxinus	confidence: 0.8	c=0.995, t=720 min, n=10	0.93	0.87	0.92	0.85
Pinus	confidence: 0.6	c=0.99999, t=720 min, n=20	0.97	0.95	0.97	0.94
Poaceae	confidence: 0.9	c=0.999999, t=720 min, n=20	0.98	0.96	0.79	0.62
Quercus	confidence: 0.99	c=0.99999, t=2880 min, n=20	0.94	0.88	0.31	0.11

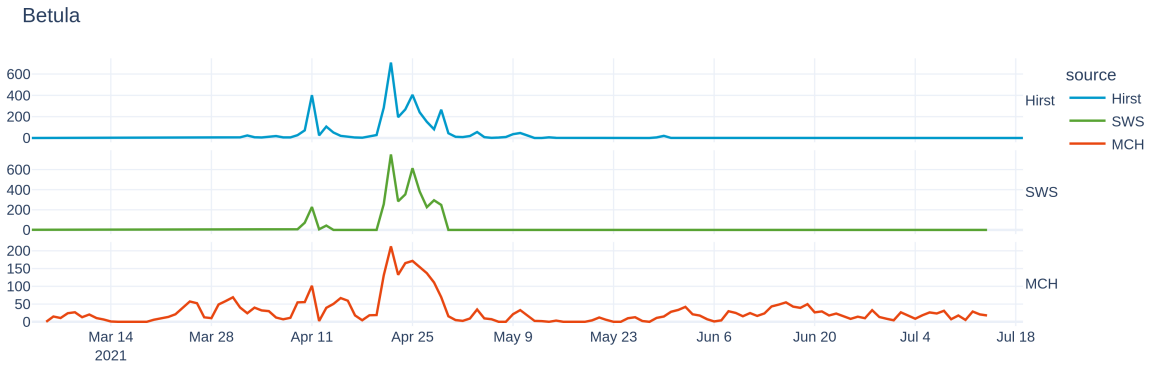


Figure 13: Betula R^2: 0.89; Betula shows very good correlation with Hirst data.

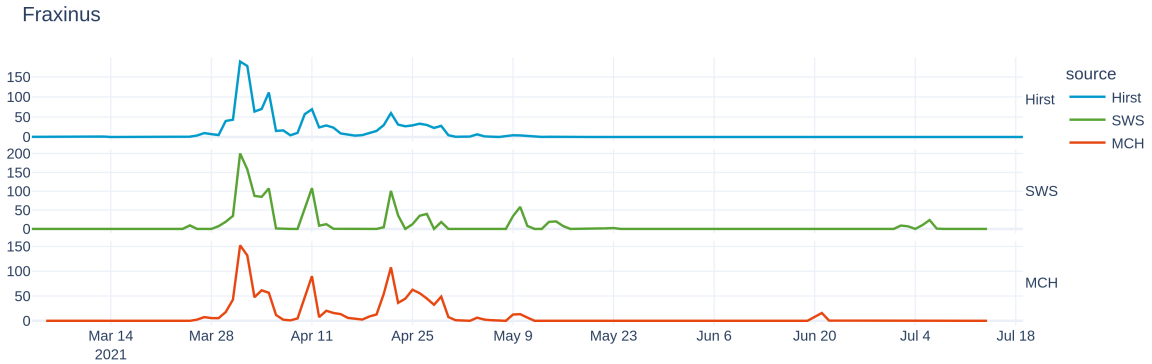


Figure 14: Fraxinus R^2: 0.87; Fraxinus shows very good correlation with Hirst data.

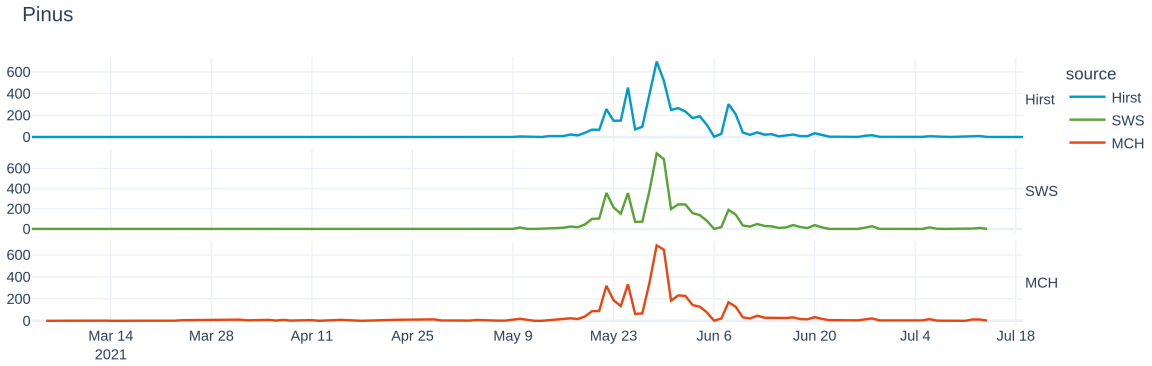


Figure 15: Pinus R^2: 0.95; Pinus shows very good correlation with Hirst data.

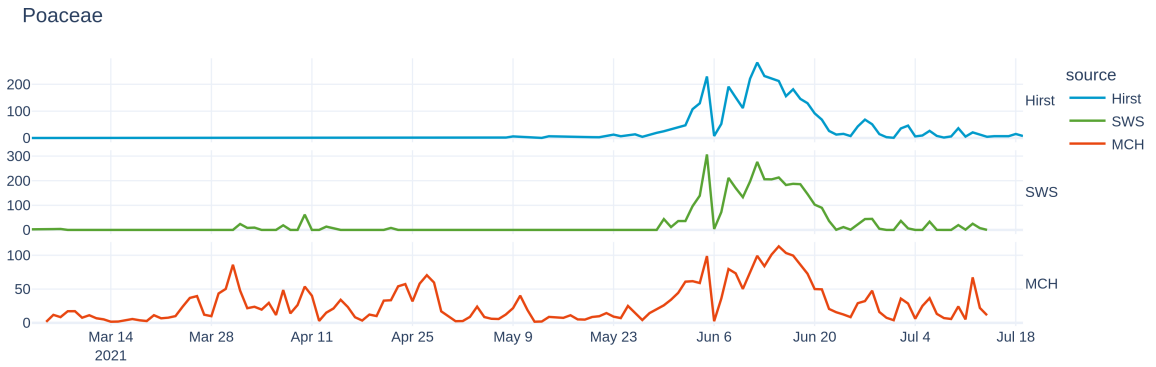


Figure 16: Poaceae R^2: 0.96; Poaceae shows very good correlation with Hirst. Off-season peaks (false-positives) are significantly reduced with the new model.

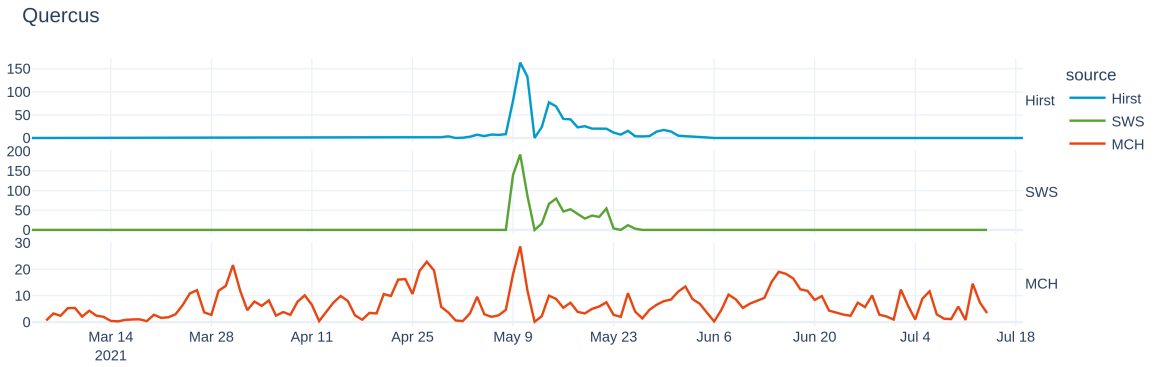


Figure 17: Quercus R^2: 0.88; Quercus shows very good correlation with Hirst data by significantly reducing off-season noise.

3 Off-Season Performance Improvements

The commonly used correlation metric often only shows a partial picture. In many cases, the absolute error in terms of concentration is just as important to show the deviation from the reference data. Here, we assess this metric using three different categories.

- Full Season: This describes the errors during the full duration of the measurement. Usually, a full year. In the case of this report, the full duration of the AutoPollen campaign.
- In-Season: The portion of the season where Hirst reported greater-than-zero concentration.
- Off-Season: The portion of the season where Hirst reported no particles.

The classification of in-season and off-season categories depends on the accuracy of Hirst measurements. In this report, we assume these measurements are reliable. However, it's important to note that Hirst measurements can have significant uncertainty at low pollen concentrations. As Adamov et al. demonstrated, concentrations below 10 pollen grains/m^3 greatly increase measurement uncertainty. For daily average total pollen concentrations, differences of over 100% were observed between three samplers studied, and for individual pollen types, differences reached up to 200% — the maximum possible for pairwise comparisons [7].

To compare the two models, this report focuses on the two pollen taxa Poaceae (Figure 16) and Quercus (Figure 17). Both classes have shown some off-season detections by the MCH model and are therefore a good test case for the new SWS model. In Figure 18, the off-season portions of the measurement period are highlighted for the Poaceae type. Ideally, we would like to see no detections in the red region. On the other hand, the algorithms should show detections in the green in-season period. Poaceae shows some early detections during mid of March. But these have low concentrations of less then one particle per cubic meter. Significant amounts start to appear around mid of May, where it quickly raises. The classification algorithms, on the other hand, show significant particle counts already at the beginning of April. While parts of it fall into periods where Hirst also detects minor concentrations, most of it is off-season (as defined above). Interestingly, both models show detections on same days, although at different levels.

Figure 19 again highlights the in and off-season periods for Quercus. Here, the MCH model reported significantly higher values than Hirst. While Hirst also had first detections at the beginning of April, larger quantities only arrived beginning of May. In contrast to the MCH model, SWS is much more in-line with Hirst. The MCH model not only missed the start of the season, it also did not align with Hirst at the end of the season. Hirst did not detect significant pollen concentrations in June, which is also what the SWS model predicted. The MCH model, however, even detected a significant peak at the start of July.

Figure 20 summarizes the performance of the MCH and SWS model with respect to mean absolute error. The concentration diagrams in Figure 18 and 19 already indicated the performance improvement. Not only did the SWS model significantly improve the off-season performance. It did so while not compromising the in-season metric.

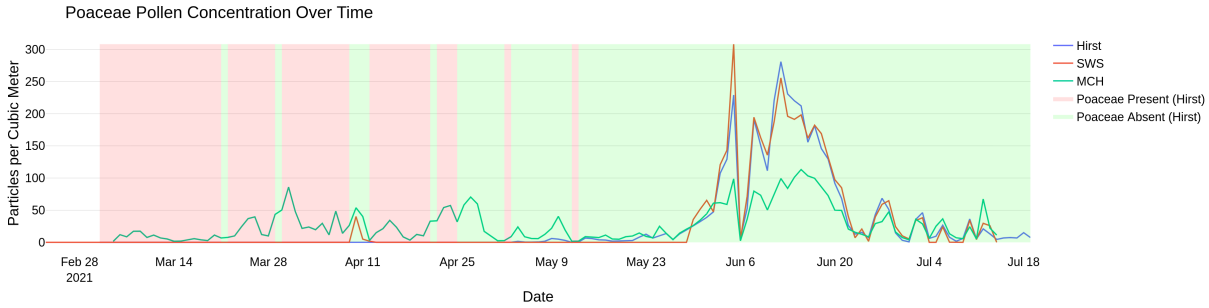


Figure 18: Poaceae concentration values for Hirst, SWS and MCH algorithms. Red and green background highlight periods where Hirst counts where greater than zero (green) or equal to zero (red)

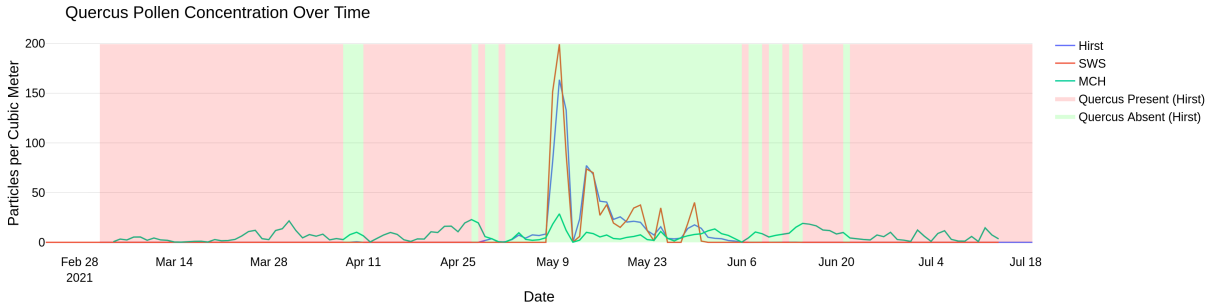


Figure 19: Quercus concentration values for Hirst, SWS and MCH algorithms. Red and green background highlight periods where Hirst counts where greater than zero (green) or equal to zero (red)

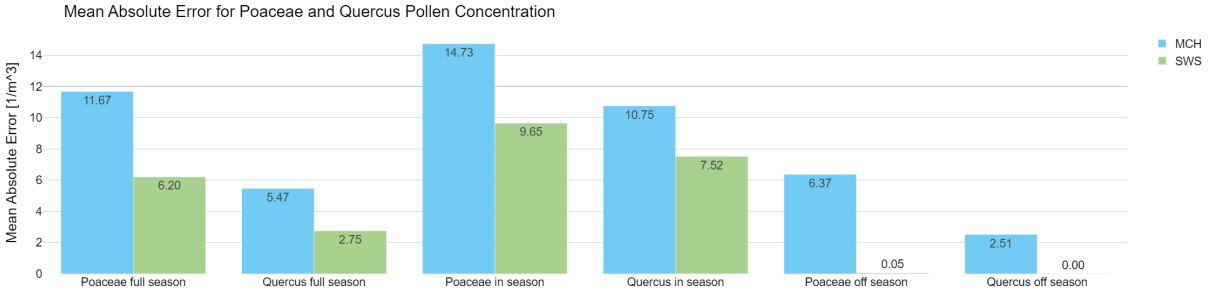


Figure 20: Performance comparison for MCH and SWS model with respect to Hirst data for the Quercus and Poaceae species. Used metric is mean absolute error. The lower the better.

4 Summary and Conclusion

The new classifier generally brings a significant improvement for the classification of the most important allergenic pollen with SwisensPoleno Mars and Jupiter instruments, as it is suitable for both types (Figure 21). The SwisensPoleno Jupiter shows an additional advantage over SwisensPoleno Mars systems for Fraxinus and Betula thanks to the complementary fluorescence measurement. This is in line with the results of Erb et. al ([5]) which showed an improvement in classification by combining the holography images with the relative fluorescence data.

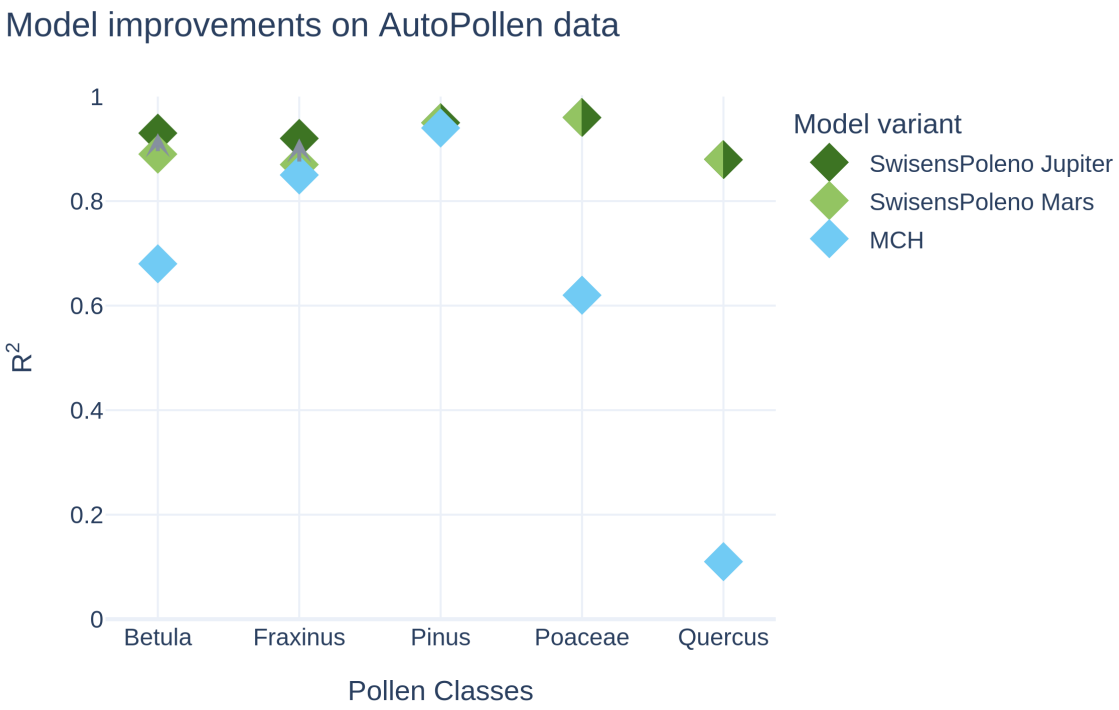


Figure 21: The new classifier performs significantly better for all SwisensPoleno instruments. Leveraging the fluorescence spectra increases the performance over using holography images for Fraxinus and Poaceae on AutoPollen data.

The classifier provides improved generalization across instruments and environments due to the wide variety of datasets used during training. Fine-tuning methods, including confidence thresholding and supervisor configuration, have been instrumental in optimizing performance by reducing off-season noise and enhancing classification confidence. Despite the complexity introduced by new classes, the overall correlation with Hirst data, especially in highly allergenic taxa, like Poaceae, is very good.

4.1 Benefits of the new classifier

- The new classifier significantly improves the classification accuracy of key allergenic pollen for both SwisensPoleno Mars and Jupiter systems.
- The average correlation to Hirst could be improved by 45.9% over the existing model, reaching R^2 values of over 0.9 for most of the relevant taxa
- The out-of-season false-positive rate is greatly reduced.
- Suppression of false-positive detections due to misclassification of water droplets as Poaceae was improved.
- Additional pollen, spores and further classes are available
  - Additional pollen taxa: Ambrosia, Artemisia, Olea, Ostrya, Parietaria, Salix, Urtica.
  - Additional spore classes: Alternaria and Phytophthora
  - Additional other particle classes: Mineral Dust (Illite-NX) and Sand.
- The new classifier uses fluorescence data as additional input but can also deal with holo data only, allowing the use of the same classifier for both SwisensPoleno Mars and Jupiter.

5 Outlook

The new classifier demonstrates significant advancements in the classification of allergenic pollen and other bioaerosols, providing a more accurate and versatile solution for real-time monitoring. However, further improvements and validations with Hirst trap data are necessary to maximize its potential and expand its applicability across diverse regions and environmental conditions.

- **Data Diversity and Quality:** The effectiveness of the classifier is heavily dependent on the availability of high-quality and diverse training datasets. Future efforts should focus on increasing the geographic and environmental variety of datasets by collaborating with additional partners and deploying SwisensPoleno instruments in underrepresented regions. Such datasets will enhance the classifier's ability to generalize across instruments and environments.
- **Validation through Robust Hirst Data:** Reliable Hirst time series remain critical to validate automatic monitoring systems. Expanding the analysis with public time series data and reducing uncertainties in manual pollen counting methods will ensure more accurate benchmarking of automatic classifiers.
- **Incorporation of Additional Measurement Modalities:** While fluorescence spectra have already improved classification performance, incorporating additional modalities such as fluorescence lifetime and polarization data could provide further gains. Using these features in future classifier versions could enhance the differentiation between particle types, particularly in challenging scenarios.

- **Dynamic Model Software:** The new software's ability to support ensemble models and advanced filtering methods introduces opportunities for dynamic model customization. Future developments could explore adaptive systems that automatically explore and recommend classifier thresholds and configurations based on regional or seasonal variations.
- **Global Collaboration:** The success of this classifier highlights the importance of collaborative efforts between institutions and countries. Expanding partnerships with research organizations, meteorological institutes, and environmental agencies will be essential to maintain progress and address emerging challenges in bioaerosol monitoring.

By addressing these areas, even better classifiers can be achieved, offering an increasingly reliable and comprehensive solution for monitoring bioaerosols and supporting critical applications, such as allergen tracking, environmental research, and public health initiatives.

6 Acknowledgments

Partners for datasets: Datasets used for training were provided by Swisens and various partners throughout Europe. We thank the Dublin City University, the University of Wroclaw, the Federal Office of Meteorology and Climatology MeteoSwiss [10], Sciensano, the University of Vienna, Umweltbundesamt Berlin and Agroscope for their contributions.

Research collaboration projects: SYLVA, **SY**stem for Rea**L**-Time Obser**V**ation of **A**eroallergens which is funded by the European Union, The Finnish Meteorological Institute and Swiss Confederation, Federal Department of Economi Affairs, Education and Research EAER and the State Secretariat for Education, Research and Innovation SERI https://sylva.bioaerosol.eu/

References

[1] Sauvageat, E., Zeder, Y., Auderset, K., Calpini, B., Clot, B., Crouzy, B., Konzelmann, T., Lieberherr, G., Tummon, F., and Vasilatou, K. (2020). Real-time pollen monitoring using digital holography. *Atmospheric Measurement Techniques*, *13*(3), 1539–1550. https://doi.org/10.5194/amt-13-1539-2020.

[2] Maya-Manzano, J. M., Tummon, F., Abt, R., Allan, N., Bunderson, L., Clot, B., Crouzy, B., Daunys, G., Erb, S., Gonzalez-Alonso, M., Graf, E., Grewling, Ł., Haus, J., Kadantsev, E., Kawashima, S., Martinez-Bracero, M., Matavulj, P., Mills, S., Niederberger, E., Lieberherr, G., Lucas, R. W., O'Connor, D. J., Oteros, J., Palamarchuk, J., Pope, F. D., Rojo, J., Šaulienė, I., Schäfer, S., Schmidt-Weber, C. B., Schnitzler, M., Šikoparija, B., Skjøth, C. A., Sofiev, M., Stemmler, T., Triviño, M., Zeder, Y., and Buters, J. (2023). Towards European automatic bioaerosol monitoring: Comparison of 9 automatic pollen observational instruments with classic Hirst-type traps. *Science of The Total Environment*, 866, 161220. https://doi.org/10.1016/j.scitotenv.2022.161220

[3] Hirst, J. M. (1952). An Automatic Volumetric Spore Trap. *Annals of Applied Biology*, *39*(2), 257–265. https://onlinelibrary.wiley.com/doi/abs/10.1111/j.1744-7348.1952.tb00904.x.

[4] M. Tan and Q. Le, "EfficientNet: Rethinking Model Scaling for Convolutional Neural Networks," in Proceedings of the 36th International Conference on Machine Learning, 2019.

[5] Erb, S., Graf, E., Zeder, Y., Lionetti, S., Berne, A., Clot, B., Lieberherr, G., Tummon, F., Wullschleger, P., and Crouzy, B. (2024). Real-time pollen identification using holographic imaging and fluorescence measurements. *Atmospheric Measurement Techniques*, *17*(2), 441–451. https://doi.org/10.5194/amt-17-441-2024.

[6] McInnes, L., Healy J., Melville, J. (2020) UMAP: Uniform Manifold Approximation and Projection for Dimension Reduction. *arXiv-Computational Geometry*, *17*(2), 441–451. https://arxiv.org/abs/1802.03426.

[7] Adamov, S., Lemonis, N., Clot, B. et al. (2024) On the measurement uncertainty of Hirst-type volumetric pollen and spore samplers. *Aerobiologia 40*, 77–91 https://doi.org/10.1007/s10453-021-09724-5

[8] Crouzy, B., Lieberherr, G., Tummon, F. et al. (2022) False positives: handling them operationally for automatic pollen monitoring. *Aerobiologia 38*, 597 https://doi.org/10.1007/s10453-022-09765-4

[9] Triviño, M.M., Maya-Manzano, J.M., Tummon, F. et al. (2023) Variability between Hirst-type pollen traps is reduced by resistance-free flow adjustment. *Aerobiologia 39*, 257–273. https://doi.org/10.1007/s10453-023-09790-x

[10] Erb, S. (2024). Pollen holographic images and light-induced fluorescence measurements at the species level. Zenodo. https://doi.org/10.5281/zenodo.13991960